Molecular Cell, Volume *73*

Supplemental Information

Architecture of Microcin B17 Synthetase: An Octameric Protein Complex Converting a Ribosomally Synthesized Peptide into a DNA Gyrase Poison

Dmitry Ghilarov, Clare E.M. Stevenson, Dmitrii Y. Travin, Julia Piskunova, Marina Serebryakova, Anthony Maxwell, David M. Lawson, and Konstantin Severinov

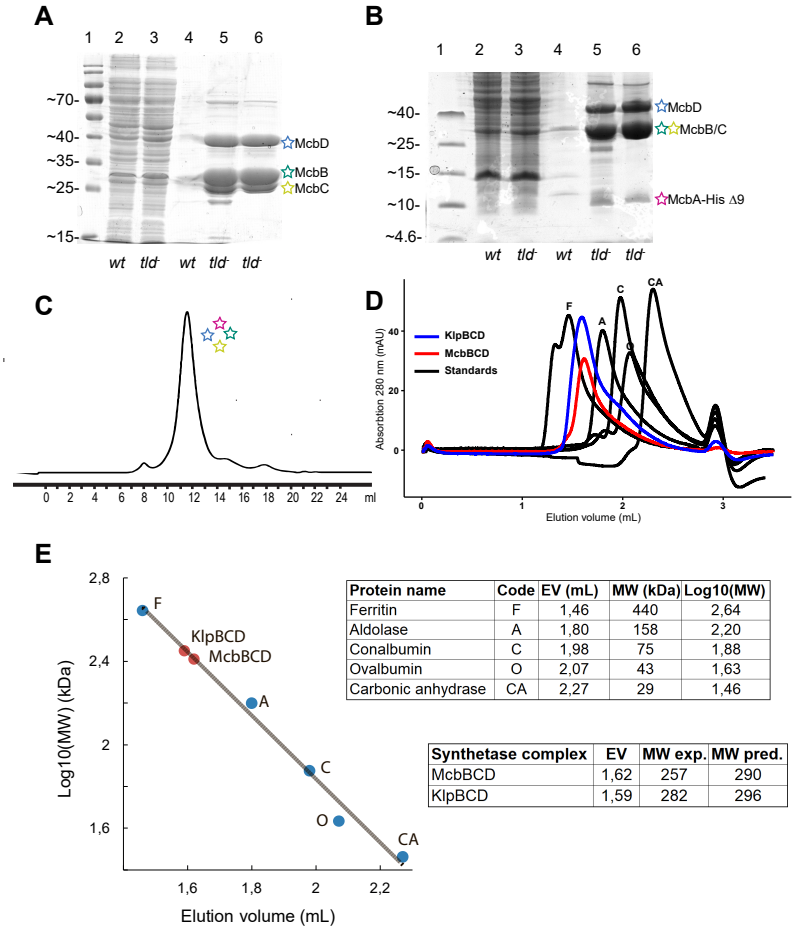

Protein name	Code	EV (mL)	MW (kDa)	Log10(MW)
Ferritin	F	1,46	440	2,64
Aldolase	A	1,80	158	2,20
Conalbumin	C	1,98	75	1,88
Ovalbumin	O	2,07	43	1,63
Carbonic anhydrase	CA	2,27	29	1,46

Synthetase complex	EV	MW exp.	MW pred.
McbBCD	1,62	257	290
KlpBCD	1,59	282	296

Supplementary Figure S1. McbBCD complex purification. Related to Figure 2

(A-C) McbBCD purification from Δ*tld* cells. A. A Tris-Glycine SDS-PAGE analysis of lysates and eluates from a Ni-NTA column. Lane 1, molecular weight marker. Lanes 2 and 3: lysates of control wild-type cells transformed with pBAD Ec-McB-His and *tld* mutant cells, respectively. Lanes 4 and 5: corresponding eluates from Ni-NTA resin. Lane 6: His-pro-MccB17-BCD complex after size exclusion chromatography (see **C**). The higher molecular weight band (ca. 70 kDa) is a contaminant. **B.** The identical samples (as A) were loaded onto a Tris-Tricine gel to resolve low MW components and a band corresponding to His-pro-MccB17 was now resolved **C.** Gel-filtration (Superdex S200 Increase 10/300) trace of affinity-purified synthetase His-pro-MccB17-BCD complex, peak fraction loaded on denaturing gels with the protein marker (**A-B**). Coloured stars indicate components of His-Pro-MccB17-BCD complex; corresponding protein bands were analysed by MALDI-MS to confirm protein identity.**(D-E) Analytical SEC of McbBCD and KlpBCD complexes. A**. FPLC traces of purified McbBCD (red), KlpBCD (blue) and molecular weight standards (black) on Superdex 200 Increase 5/150. **B**. Calibration curve and M_w calculation for both BCD complexes.

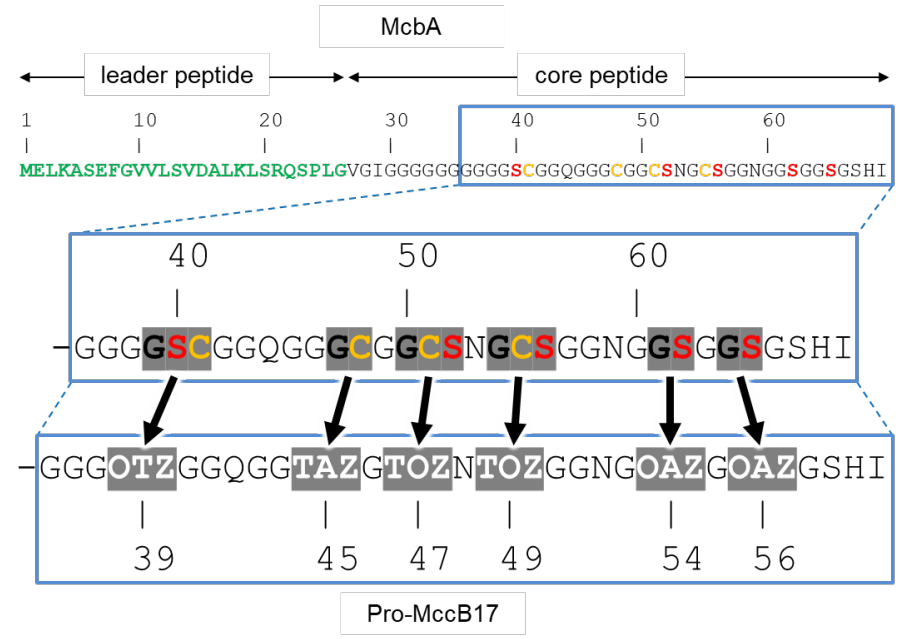

OAZ = oxazole – derived from Gly-Ser
TAZ = thiazole – derived from Gly-Cys
OTZ = oxazole-thiazole – derived from Gly-Ser-Cys
TOZ = thiazole-oxazole – derived from Gly-Cys-Ser

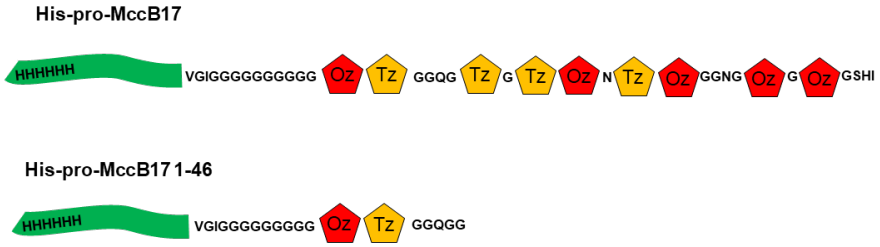

Supplementary Figure S2. Nomenclature used for pro-MccB17 in McbBCD structures. Related to Figures 1 and 2

For the building and refinement of fragments of pro-MccB17 we treated the mono- and bis-heterocycles as pseudo-amino acids, which could then be incorporated into peptide fragments between standard amino acids. However, this affected the sequence numbering because the modifications conflate either two or three amino acids into one pseudo-amino acid, such that the final product becomes nine residues shorter. The revised numbering scheme is shown. Below are shown two peptide ligands used to obtain crystal structures, a full-length modified His-tagged McbA peptide and a truncated (McbA 1-46) peptide.

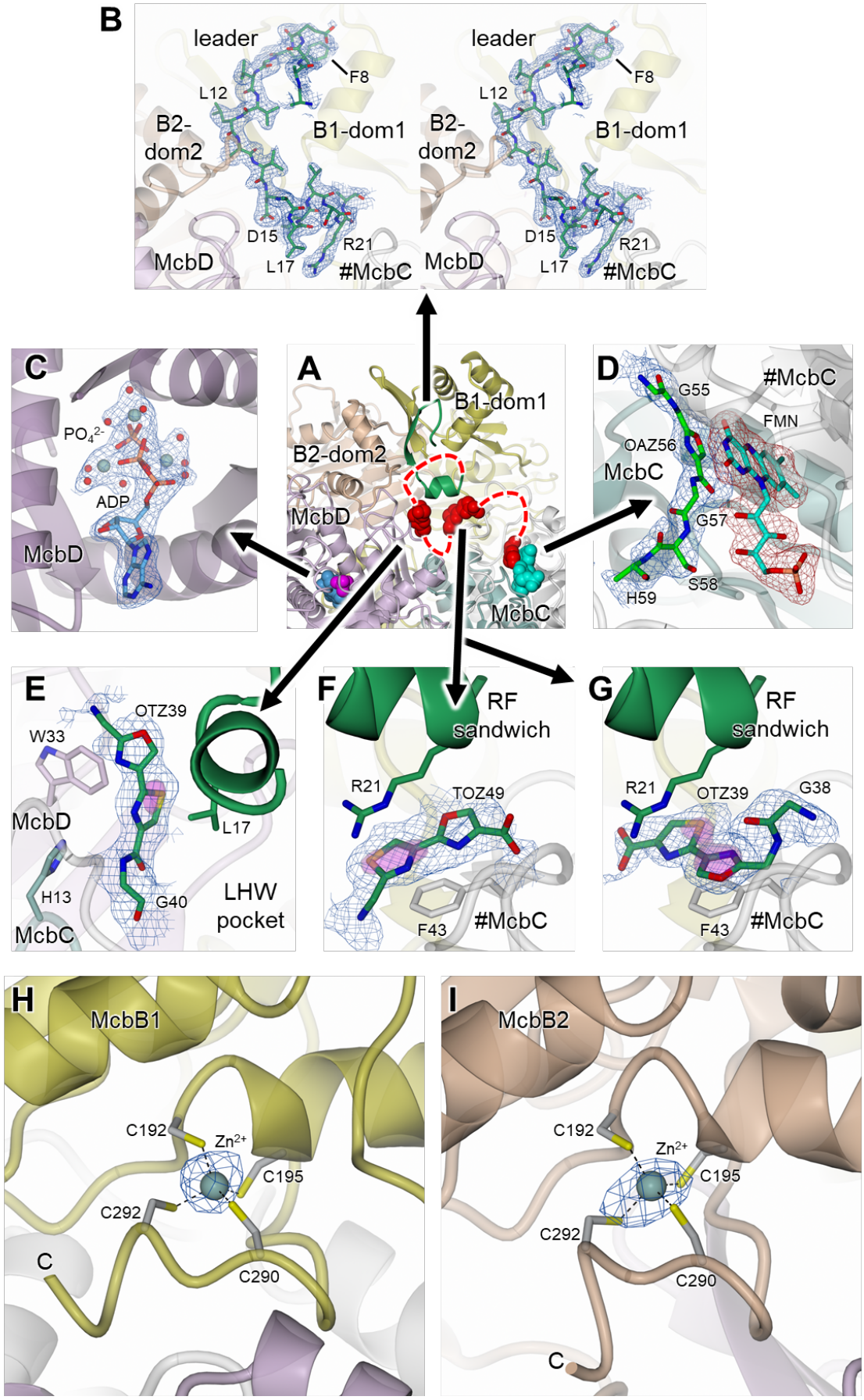
B
leader
F8
L12
B2-dom2
B1-dom1
D15
R21
McbD
L17
#McbC
leader
F8
L12
B2-dom2
B1-dom1
D15
R21
McbD
L17
#McbC
C
PO_4^{2-}
ADP
McbD
A
B1-dom1
B2-dom2
McbD
McbC
D
G55
#McbC
FMN
OAZ56
McbC
G57
S58
H59
E
OTZ39
W33
McbD
L17
H13
G40
LHW pocket
McbC
F
RF sandwich
R21
TOZ49
F43
#McbC
G
RF sandwich
R21
OTZ39
G38
F43
#McbC
H
McbB1
C192
Zn^{2+}
C195
C292
C
C290
I
McbB2
C192
Zn^{2+}
C195
C292
C290
C

Supplementary Figure S3. Omit difference density maps and anomalous difference Fourier map for zinc sites. Related to Figure 2

Omit mF_{obs}-DF_{calc} difference electron density maps were generated for the bound ligands using phases from the final models without the ligands after the application of small random shifts to the atomic coordinates, re-setting temperature factors, and re-refining to convergence. **A**. Overview of sites represented in the rest of the figure, shown in the standard view (as in **Figure 2C**). **B**. Stereoview of density for the leader peptide in BCD-pB17 with key residues labelled (2.1 Å resolution omit density contoured at ~2.0 σ). **C**. Density for ADP and phosphate together with associated magnesium ions and waters in BCD-pB17-ADP-P (2.35-Å resolution omit density contoured at ~3.5 σ). **D**. Separate omit maps calculated for the product (blue mesh) and FMN (red mesh) in the McbC active site of BCD-pB17 (both calculated at 2.1-Å resolution and contoured at ~2.0 σ). **E**. Density for the OTZ39-Gly40 ligand in the LHW pocket of BCD-pB17 [2.1 Å resolution omit density contoured at ~2.0 σ (blue mesh) and ~6.0 σ (magenta transparent surface)]. **F**. Density for the TOZ49 ligand in the RF sandwich of BCD-pB17 [2.1-Å resolution omit density contoured at ~1.8 σ (blue mesh) and ~6.0 σ (magenta transparent surface)]. **G**. Density for the Gly38-OTZ39 ligand in the RF sandwich of BCD-pB17short [1.85-Å resolution omit density contoured at ~2.0 σ (blue mesh) and ~5.0 σ (magenta transparent surface)]. **H-I.** An additional BCD-pB17 data set (not shown) was collected at the zinc *K* X-ray absorption edge (λ = 1.283 Å) at a resolution of 2.7 Å. This was used to calculate an anomalous difference Fourier map with phases derived from the final BCD-pB17 model. **H** and **I** show clear peaks for the two structural zinc ions in the asymmetric unit, one in each McbB subunit (map contoured at ~4.0 σ).

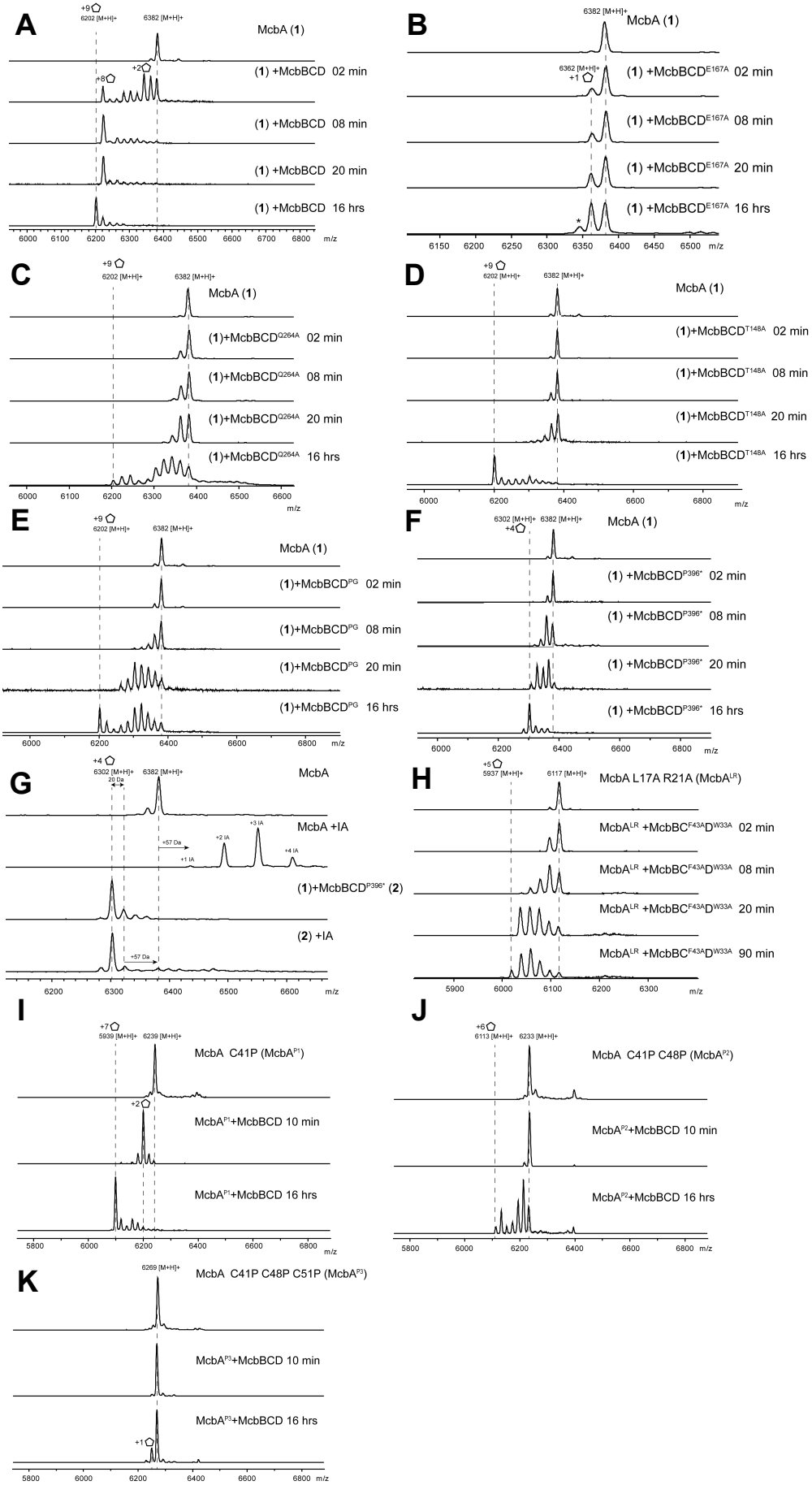
A
McbA (1)
(1) +McbBCD 02 min
(1) +McbBCD 08 min
(1) +McbBCD 20 min
(1) +McbBCD 16 hrs
B
McbA (1)
(1) +McbBCDE167A 02 min
(1) +McbBCDE167A 08 min
(1) +McbBCDE167A 20 min
(1) +McbBCDE167A 16 hrs
C
McbA (1)
(1)+McbBCDQ264A 02 min
(1)+McbBCDQ264A 08 min
(1)+McbBCDQ264A 20 min
(1)+McbBCDQ264A 16 hrs
D
McbA (1)
(1)+McbBCDT148A 02 min
(1)+McbBCDT148A 08 min
(1)+McbBCDT148A 20 min
(1)+McbBCDT148A 16 hrs
E
McbA (1)
(1)+McbBCDPG 02 min
(1)+McbBCDPG 08 min
(1)+McbBCDPG 20 min
(1)+McbBCDPG 16 hrs
F
McbA (1)
(1) +McbBCDP396* 02 min
(1) +McbBCDP396* 08 min
(1) +McbBCDP396* 20 min
(1) +McbBCDP396* 16 hrs
G
McbA
McbA +IA
(1)+McbBCDP396* (2)
(2) +IA
H
McbA L17A R21A (McbALR)
McbALR +McbBCF43AΔW33A 02 min
McbALR +McbBCF43AΔW33A 08 min
McbALR +McbBCF43AΔW33A 20 min
McbALR +McbBCF43AΔW33A 90 min
I
McbA C41P (McbAP1)
McbAP1+McbBCD 10 min
McbAP1+McbBCD 16 hrs
J
McbA C41P C48P (McbAP2)
McbAP2+McbBCD 10 min
McbAP2+McbBCD 16 hrs
K
McbA C41P C48P C51P (McbAP3)
McbAP3+McbBCD 10 min
McbAP3+McbBCD 16 hrs
m/z

Supplementary Figure S4. Mass-spectrometry data. (Related to Figure 5)

McbBCD heterocyclisation reactions. For each reaction, 10 μM of peptide and 1 μM of enzyme were mixed and incubated at 37°C. Aliquots were taken at the indicated time points, quenched and analysed by MALDI for heterocycle formation. A 20 Da mass loss corresponds to the formation of one azole. In each case, the maximum number of detected heterocycles after overnight incubation is indicated.

A. Time-course of McbA modification by *wt* McbBCD.

B. Time-course of McbA modification by McbBCD^{E167A}. An asterisk denotes laser-induced (-15 Da) MALDI artefact.

C. Time-course of McbA modification by McbBCD^{Q264A}.

D. Time-course of McbA modification by McbBCD^{T148A}.

E. Time-course of McbA modification by McbBCD^{PG} (P394G P396G).

F. Time-course of McbA modification by McbBCD^{P396*} (P396*).

G. Evidence that McbBCD^{P396*} produces a 4-thiazole containing intermediate. An incubation of a *wt* McbA peptide (**1**) with iodoacetamide (IA) produces a mixture of 1 to 4 IA adducts (+57 Da mass shift), corresponding to the maximum number of Cys residues in the precursor. A treatment of (**1**) with McbBCD^{P396*} yields a 4-cycle-containing compound (**2**). (**2**) cannot be further labelled with IA, indicating that all four cysteines in (**2**) are cyclised. Shown is MALDI analysis of reaction products.

H. Time-course of McbA^{LR} modification by McbBC^{F43A}D^{W33A}.

I-K. Time-courses of modification of McbA Pro mutants. A Cys41Pro (**i**), Cys41Pro Cys48Pro (**j**) or Cys41Pro Cys48Pro Cys51Pro (**k**) precursor peptides were incubated with McbBCD for indicated periods of time and reaction products analysed with MALDI. Maximum number of heterocycles detected is indicated.

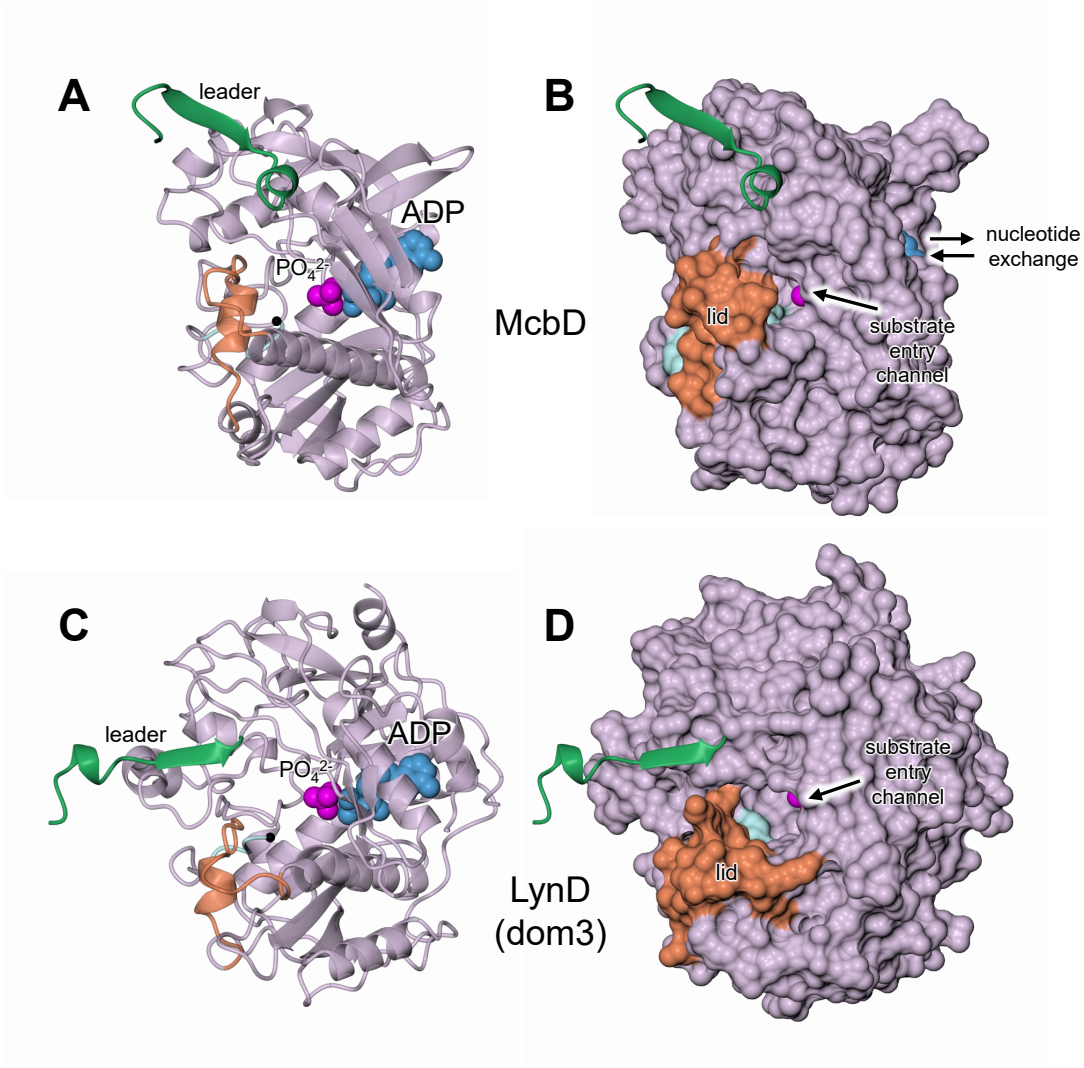

Supplementary Figure S5. Further detail of the McbD structure. Related to Figure 5

A and **B** show the isolated McbD subunit (from the side with respect to the standard view, which is shown in **Figure 5**) in cartoon and molecular surface representations. Also shown is the relative position of the leader peptide (green) and, as van der Waals spheres, the bound ADP (blue) and phosphate (magenta). The lid region (orange) and C-terminal tail (cyan) partially occlude the active site, although the phosphate is just visible through a pore that we designate the entry channel. **B** and **C** show corresponding views of domain 3 of LynD. Here the lid adopts a more open conformation allowing less restricted access to the active site.

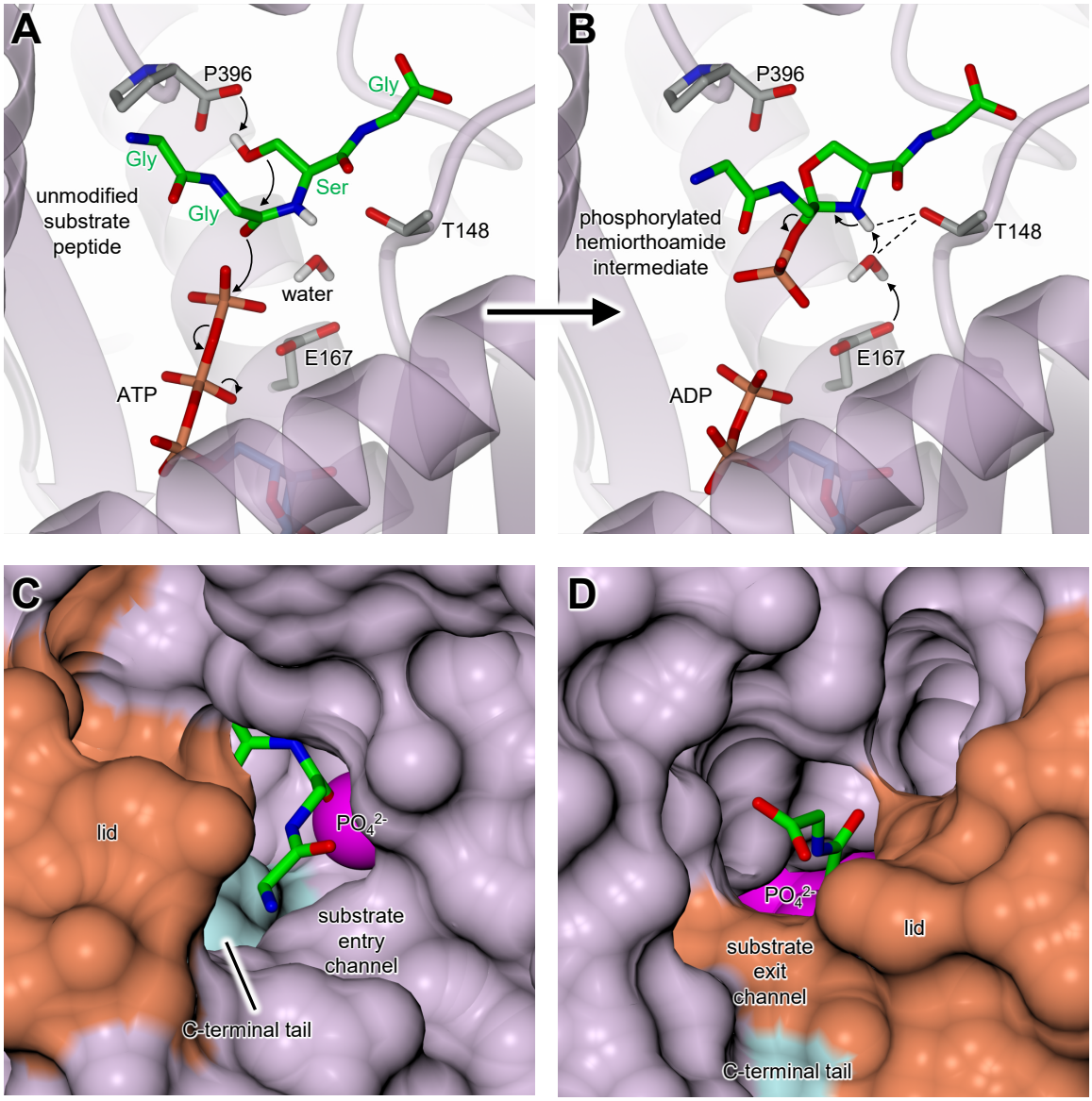

Supplementary Figure S6. Modelling of complexes with substrate and intermediate. Related to Figure 5 and STAR Methods

A and **B** show modelled substrate and intermediate complexes of McbD, respectively, starting from a Gly-Gly-Ser-Gly peptide. Also shown are key McbD residues, including Pro396 and Thr148, where mutations to both have deleterious effects on catalysis. The proposed mechanism for heterocyclization involves two bases (**Figure 5F**). We postulate that Pro396 is the first of these, but that Thr148 is not an obvious candidate for the second. Instead, we propose that a water molecule performs this role after deprotonation by Glu167. The latter was not mutated as it is also a magnesium ligand. We further suggest that Thr148 is important for the correct positioning of this water and possibly also has a role in substrate binding. **C** and **D** show how the N-terminal and C-terminal ends of the docked substrate (shown in panel **A**) are directed towards the entry and exit channels of McbD, respectively.

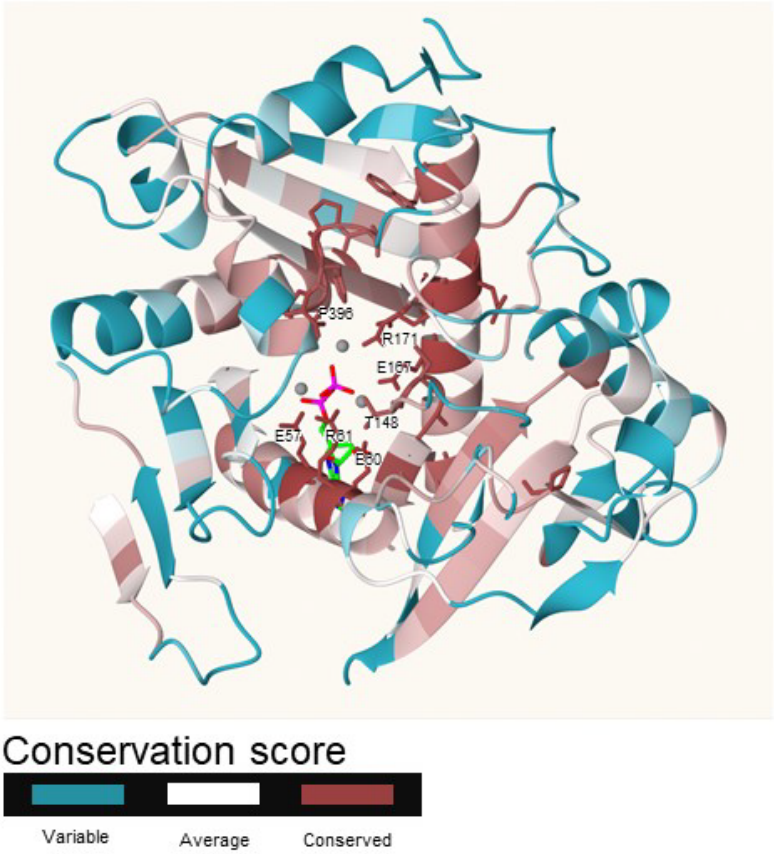

Supplementary Figure S7. Conserved amino-acid residues in the vicinity of the McbD active centre. Related to Figure 5 McbD model was submitted to ConSurf (http://consurf.tau.ac.il/) server. A HMMER search for homologous templates was performed using UNIREF90 database to construct final multiple sequence alignment. Calculated conservation scores were used to paint a cartoon representation of McbD structure with most conserved amino-acids shown as tan cylinders and labelled in the figure. Also shown are ADP and three magnesium ions.

Supplementary Table S1. Site occupancy in McbBCD structures. Related to Table 2

Structure	Treatment	Peptide clamp	LHW pocket	RF sandwich	McbC active site	McbD active site	Adjacent to R199 and R203 (McbB1)*	Crystal contact adjacent to T91 (McbB2)*
BCD-pB17	as isolated	K4-Q22	OTZ39-G40	TOZ49	G55-OAZ56-G57-S58-H59	glycerol	sulphate	unassigned density
BCD-pB17-ADP-P	as isolated, co-crystallised with ATP	A5-R21	unassigned density	Unassigned density	OAZ56-G57-S58-H59	ADP, phosphate, 3 x Mg^{2+}	sulphate	ATP (0.5 occupancy)
BCD-pB17short	as isolated with truncated pro-MccB17	K4-Q22	unassigned density	OTZ39	ethylene glycol,	glycerol	sulphate	unassigned density
BCD-free	TldD/E-treated – no pro-MccB17	M213 (McbB2) moves into site occupied by L12 of leader	unassigned density	empty	sulphate	empty	sulphate	empty

*Probably not a biologically relevant site

N.B. for each structure the asymmetric unit contains one FMN cofactor (in the McbC active site) and two Zn^{2+} ions (one associated with each copy of McbB).

Supplementary Table S2. Oligonucleotides used in this study. Related to STAR Methods

Name	Sequence	Purpose
McbANcoHis	AATTTACCATGGGACATCACCATCACCATCATATGG AATTAAAAGCGAGTGA	Construction of pBAD Ec-McB-His
McbASmaRev	TTAACCCGGGCATTACTGAAAAGATGTGGAAC	
46stopF	GGTCAAGGTGGCTGATGTGGTGGTTGC	Construction of pBAD Ec-McB-His 1-46
46stopR	GCAACCACCACATCAGCCACCTTGACC	
McbB_pBAD_HisB_XhoI_F	ATATACTCGAGCATGGTGCTCCCTGATATTAAAAAA GGAAAAG	Subcloning of *mcbBCD* fragment to produce pBAD mcbBCD
McbD_pBAD_HisB_EcoRI_R	ATATAGAATTCTTATGGGAATGGTACCATCTTTGATTCTC	
McbA_L17A_R21A_F	TGCTAAATTATCAGCCCAGTCTCCATTAGGTGTTGG	Mutagenesis of *mcbA* and cloning of mutated genes into pET28MBP vector
McbA_L17A_R21A_R	TGGGCTGATAATTTAGCAGCATCAACGGACAAAAC	
McbA_C41P_F	GGCGGCGGCGGTAGCCCGGGTGGTC	
McbA_C41P_R	GACCACCCGGGCTACCGCCGCCGCC	
McbA_C48P_C51P_F	TGGCGGTCCTGGTGGTCCGAGCAACGGT	
McbABamFor	TAATATGGATCCATGGAATTAAAAGCGAGTG	
McbANotRev	TAATATGCGGCCGCTCAGATATGTGAACCACTT C	
McbD_E167A_F	AGGTTCCTTGTGTGCATTTATGG	Mutagenesis of McbD
McbD_E167A_R	CCATAAATGCACACAAGGAACC	
McbD_Q264A_F	TTGTGGGCATCGTATATATGCC	
McbD_Q264A_R	GCATATATACGATGCCCACAATTCC	
McbD_W33A_R	ATACGCTCATAGTCCGCTATCTGAGAAAACG	
McbD_W33A_F	CAACGTTTTCTCAGATAGCGGACTATGAGCG	

McbD_T148A_R	CTACATCCGCATGCATCTCTGTCAGG	
McbD_T148A_F	CTGACAGAGATGCATGCGGATGTAG	
McbD_minusPro_EcoR1_R	ATATAGAATTCTTAGAATGGTACCATCTTTGAT TCTCTGAC	
McbD_PtoG_EcoR1_R	ATATAGAATTCTTATCCGAATCCTACCATCTTT GATTCTCTGACTTTAATAC	
McbC_F43A_R	CGCGGACACGGCAGTTCGTTCAGC	Mutagenesis of McbC
McbC_F43A_F	GCTGAACGAACTGCCGTGTCCGCG	
Y202Af	TGAAAAAGCTTTGTTCAAAGCACGCTACAGAG	
Y202Ar	CTCTGTAGCGTGCTTTGAACAAAGCTTTTTCA	